Journal of

Mechanics of Materials and Structures

EFFECT OF TIP PROFILE ON CUTTING PROCESSABILITY OF A TRAPEZOIDAL CUTTING BLADE INDENTED TO AN ALUMINUM SHEET

Seksan Chaijit, Shigeru Nagasawa, Yasushi Fukuzawa,
Mitsuhiro Murayama and Isamu Katayama

Volume 1, Nº 8 *October 2006*

mathematical sciences publishers

JOURNAL OF MECHANICS OF MATERIALS AND STRUCTURES
Vol. 1, No. 8, 2006

EFFECT OF TIP PROFILE ON CUTTING PROCESSABILITY OF A TRAPEZOIDAL CUTTING BLADE INDENTED TO AN ALUMINUM SHEET

SEKSAN CHAIJIT, SHIGERU NAGASAWA, YASUSHI FUKUZAWA, MITSUHIRO MURAYAMA AND ISAMU KATAYAMA

This paper is an investigation of detaching phenomena of a trapezoidal cutting blade on a wedged surface of a thin work sheet. To study critical conditions for cutting off an aluminum sheet, the wedged profile of the work sheet was experimentally studied by varying the tip thickness of the trapezoidal cutting blade, which simulated a crushed bevel blade. To analyze the detached condition and separation force of the wedged sheet, an elastoplastic finite element program was used to analyze wedge indentation to the work sheet. The following results were obtained: (i) the deformation of the wedged sheet can be classified in four patterns; (ii) the critical condition for cutting off the work sheet depends on the ratio of tip thickness by sheet thickness w/t; (iii) the separation of the work sheet occurred statistically for $w/t = 0.13 \sim 0.28$; and (iv) the separation line force can be used to explain the necking mode and the detached condition.

1. Introduction

A cutting method in which a center bevel blade cuts into sheet material on a counter plate is widely used in the packaging or printing industry, for example, diecutting of paperboard, labels, laminated resin sheets, ductile metal film, and other similar materials [Inaba 1998; Hesse and Tenzer 1963; Tanaka and Akamatsu 2001]. However, many problems that affect product quality are caused by the variation of blade tip such as crushing or abrasion of the wedge profile during the cutting process. These problems occur because in a flatbed type cutting machine, the cutting blade moves reciprocally and contacts with the counter plate without any stopper. [Grebe and Hofer 1973] experimentally studied the relationship between the blade abrasion and its cutting force variance for both paperboards and corrugated boards. [Nagasawa et al. 2001; Nagasawa et al. 2004] investigated experimentally and numerically how the tip profile of a normal blade was crushed during cutting of a white-coated paperboard. It was shown that the cutting blade tip became trapezoidal (as a crushed form) when the cutting blade tip contacted with the counter plate. [Nagasawa et al. 2002] also reported on the effects on tip shape when string-like dust occurs, and on the relationship between breaking characteristics of paperboard and cutting force responses. These results indicated to us that study of the processability of the trapezoidal cutting blade would be of interest.

Several theoretical works [Grunzweig et al. 1954; Hill 1953] on wedge indentation into an isotropic plastic body are useful to understand the influence of friction, apex angle of the bevel blade, thickness of the work piece, and yield stress of the work piece on the indentation force. However, these traditional models were not sufficient to explain the profile effect of the crushed tip on the die cutting process. [Murayama et al. 2003; 2004] have reported on the load response of wedge indentation into a thin

Keywords: shear cutting, detaching, elastoplastic FEM, separation force, wedge indentation, upsetting.

aluminum sheet, by using a trapezoidal cutting blade having a flat region on the tip to simulate crushing. In that study, Murayama et al. found the second necking mode through FEM simulation and experimental cutting of an aluminum sheet, where the ratio of tip thickness w of the blade and the thickness t of the work sheet was $w/t = 0.013 \sim 0.23$. That result contributed to an explanation of how burrs of an aluminum sheet occur beneath the blade tip. The mechanism that generates the aluminum burrs seems to be similar to the one which generates string-like chips on white-coated paperboard. The occurrence of necking on the bottom surface of the worksheet depended on w/t.

When w/t becomes relatively large ($w/t \gg 0.1$), the sliding surface of the wedge blade is prone to detach from the deformed work sheet, and the blade tip generally pushed the work sheet in an upsetting mode. However, the critical condition for wedge separation from the work sheet was not analyzed sufficiently for $w/t > 0.3$. However, thinner sheets, that is, those less than 15 μm thickness with respect to the tip thickness of 5 μm, are often required in pattern diecutting of resin sheets or thin metal sheets. In addition, the detaching condition on the sliding surface of the trapezoidal bevel blade, and the separation force of the wedged sheet were not covered.

In this paper, therefore, we analyzed the trapezoidal blade indentation into an aluminum sheet both numerically and experimentally for the range of $0.036 < w/t < 0.64$. To investigate the variance of cutting processability of the blade indented on the work sheet and the critical condition for cutting off the work sheet, we focused on the final separation stage of the worksheet in the pushing shear process. In addition, the detaching phenomenon between the blade surface and the deformed work sheet has also been discussed with respect to the separation line force. It seems that the critical condition and the detaching mechanism would be useful for designing a new blade profile or modifying the crushed blade tip.

This paper is laid out as follows: Section 2 describes the experimental method and the simulation conditions. Section 2.1 includes details of the experimental method and the material properties of specimen, and Section 2.2 includes details about the finite element modeling and its conditions. A simulation model and several parameters with respect to the detaching phenomena are also introduced. Section 3 presents results and discussion regarding wedge indentation to the work sheet. Section 3.1 covers the relationship between the resistance of blade indentation and w/t. Section 3.2 presents corresponding results for the deformation shape and the separation probability of the aluminum work sheet through varying w/t. Section 3.3 and Section 3.4 cover the detaching phenomena on the sliding surface of the wedge blade, and the effect of friction coefficients, respectively. Section 3.5 gives the stress distribution around the blade tip on the final stage of indentation. Section 3.6 presents critical conditions and worksheet deformation patterns that were derived both from detaching phenomena on the wedge surface, and from the load response. Section 3.7 covers numerical results regarding the separation line force of the wedged worksheet. Finally, in Section 4, we draw conclusions.

Nomenclature

B	Width of specimen, mm
D	Lower crosshead displacement, mm
E	Young's modulus, GPa
F	The plastic coefficient, MPa

F_v	Force applied in vertical to the cuter blade, kN
K_v	Equivalent spring constant of the apparatus, kN/m/mm
L	Length of specimen in the rolling direction, mm
V	Lower crosshead velocity, mm/min
a_c	Contact length, mm
a_d	Detached length, mm
d	Indentation depth , $d = (D - Fv/K_a)$, mm
d_{co}	Upper-bound position depth of the detaching phenomena in the complete open position
d_{so}	Lower-bound position depth of the detaching phenomena in an open start position.
k	Shearing yield stress ($\approx \sigma_{0.2}/\sqrt{3}$)
n	Work-hardening exponent
p	Probability of separation, %
p_m	Normal pressure on the wedge surface of the cutting blade
t	Thickness of work sheet, mm
w	Tip thickness of cutting blade, μm
f	Cutting line force, $f = Fv/B$, kN/m
f_1	First inflection of cutting line force
f_1'	First inflection of cutting line force for $w/t > 0.23$
f_s	Lateral component of the applied line force, called as the separation line force , kN/m
α	Bevel apex angle, degrees
$\sigma_{0.2}$	Proof stress of the work sheet, MPa
σ_B	Ultimate tensile strength of the work sheet, MPa
$\tau_{\max}$	Maximum shear stress, MPa
σ_{pmax}	Maximum principal stress, MPa
μ_C	Friction coefficient between the cutter blade and the work sheet
μ_P	Friction coefficient between the work sheet and the counter plate

Subscripts

B	denotes breaking
c	denotes contact condition
d	denotes detached condition
max	denotes maximum
n	denotes necking
s	denotes separation line force
u	denotes the local minimum point after breaking

2. Experimental and simulation methods

Since the cutting mechanism of the pushing shear process is assumed to be primarily characterized by the ratio of tip thickness to the sheet thickness w/t, the cutting line force f kN/m, which is applied

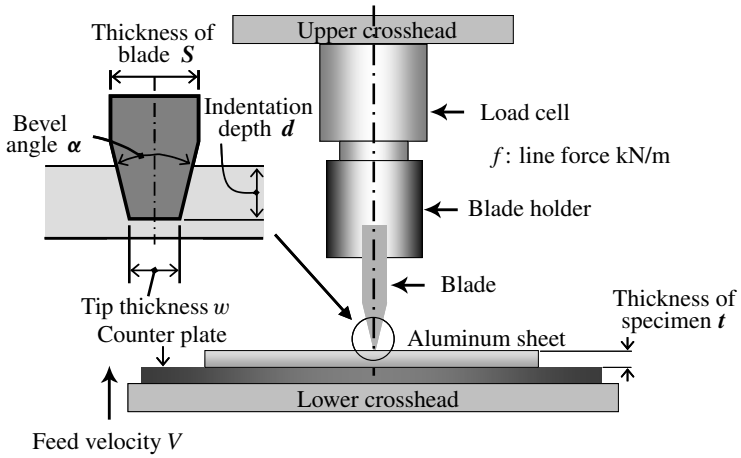

Figure 1. Schematic of experimental apparatus.

vertically to the cutting blade, and the contact condition on the blade surface or on the counter plate were investigated by varying the ratio of the indentation depth and the sheet thickness d/t with respect to w/t.

2.1. ***Experimental method and specimen.*** For the indentation experiment, we used a commercially available aluminum sheet (JIS-A1050P) of 0.39 mm thickness. Specimens were rectangle sheets with length in the rolling direction $L = 50$ mm and width $B = 20$ mm. Tensile properties of the sheet materials for both the longitudinal and transverse direction are shown in Table 1. The work hardening characteristic, that is, the stress-strain relation of the material, was approximated by the power law expression $\sigma = F\varepsilon^n$, where F is the plastic coefficient, ε is the equivalent plastic strain and n is the work-hardening exponent. In this study, we mainly considered the rolling direction of the material's behavior. The trapezoidal bevel blades had a length of 40 mm, thickness $S = 0.9$ mm, bevel apex angle $\alpha = 42$ degree, and tip hardness of 600 HV. The tips of the blades we used were filed using emery papers to tip thicknesses $w = 14, 31, 54, 71, 92, 129, 166, 200$ and $250\,\mu$m. Non-filed cutters had an average thickness of $w = 5\,\mu$m.

Properties	RD	CD
Young's modulus E [GPa]	76	76
Proof stress $\sigma_{0.2}$ [MPa]	115	140
Ultimate tensile strength σ_B [MPa]	125	150
Plastic coefficient F [MPa]	160	224
Work-hardening exponent n	0.07	0.08

Table 1. Mechanical properties of aluminum sheet (A1050P). RD is the rolling direction; CD the cross direction.

Figure 1 shows a schematic of the experimental apparatus. Measurements were carried out five times for each thickness w. The position of the cutter blade was vertical to the surface of the aluminum sheet, while the cross-angle between the rolling direction of the aluminum sheet and the longitudinal direction of the cutting blade was 90 degrees. On the experimental apparatus (universal testing equipment) the upper crosshead had a trapezoidal bevel center blade mounted on a load cell with maximum load of 5 kN.

Each specimen of the aluminum sheet was placed onto the counter plate fixed on the lower crosshead. The lower crosshead moved upward with a velocity $V = 0.05$ mm/min. The indentation depth of the cutting blade into the specimen was estimated using the relation $d = (D - F_v/K_v)$, where K_v kN/m/mm is an equivalent spring constant of the apparatus, D mm is the lower crosshead displacement, and F_v kN/m is the line force applied in vertical to the cutting blade.

To ensure nonlubricated contact between the specimen and the counter plate, the tool surface was washed with alcohol before indenting. A previous experiment [Murayama et al. 2004] revealed that with the horizontal method based on JIS-P8147 the average friction coefficient μ_C between the cutting blade and the specimen was 0.20 (max .0.28 $\sim$ min .0.18), and the average friction coefficient μ_P between the specimen and the counter plate was 0.25 (max .0.28 $\sim$ min .0.20).

2.2. ***Simulation method.*** A commercial finite element program, MSC.MARC [MSC 2003], using an updated Lagrange procedure and large strain was used to simulate the trapezoidal cutting blade indentation on an aluminum sheet. Figure 2a shows a schematic illustration of the simulation model, in which the aluminum sheet was considered as a deformable body and modeled as the right-hand half symmetry of a rectangle of 4.0 mm in length. The cutting blade and the counter plate were modeled as rigid contact bodies. The finite element meshes of the deformed body consisted of 17,000 four-node quadrilateral elements with minimum side length of 5 μm. The element type was considered to be plain-strain quadrilateral with four-point Gaussian integration. The coulomb friction model was assumed for each contact surface, since no sticking slip was observed clearly during the simulation of blade indentation into the aluminum sheet. The deformable body was assumed to be an isotropic, elastoplastic material obeying the isotropic hardening power law $\sigma = F\varepsilon^n$. The value of $F = 160$ MPa and $n = 0.07$ were chosen as described in previous section. Because of locally large deformation during the pushing process, a globally automatic re-meshing criterion with overlay meshing method was used. Elements were assumed to have no crack and no fracture during the cutting process. For the tip profile of the trapezoidal cutting blade and the friction coefficients, we chose parameters as shown in Table 2. Corner radii were assumed to be

Tip thickness: $w = 0, 10, 30, 50, 70, 90, 120, 150, 180, 200, 250\,\mu$m
Sheet thickness: $t = 0.4$ mm.
Bevel apex angle: $\alpha = 42°$
Friction coefficient of trapezoidal blade: $\mu_c = 0, 0.1, 0.2, 0.4$
Friction coefficient of counter plate: $\mu_p = 0, 0.1, 0.2, 0.4$

Table 2. Simulation parameters for blade indentation.

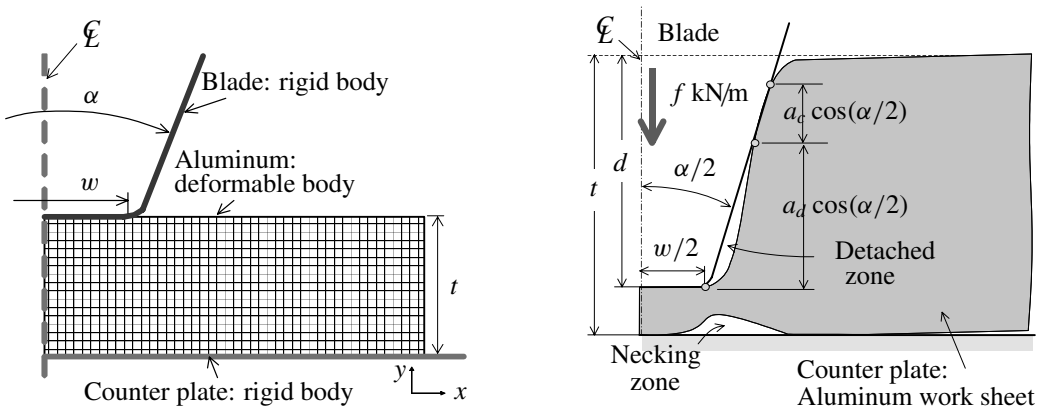

(a) Initial profile (b) Indentation profile

Figure 2. Simulation model with respect to detaching phenomena on the wedge surface.

5 μm on both sides. From the experimental result of friction coefficients μ_C, μ_P, dispersion was roughly 0.1. therefore, the friction coefficients μ_C, μ_P were initially assumed to be 0.2.

Figure 2b schematically illustrates a deformed sheet with respect to the occurrence of a detached surface. When the blade was indented on the work sheet, a detached length a_d and a contact length a_c on the sliding surface of the blade were evaluated as shown in Figure 2. Where, a_d is defined as the projection length on the blade surface which is detached from the work sheet, while a_c is defined as the projection length on the blade surface which contacts with the worksheet.

3. Results and discussion

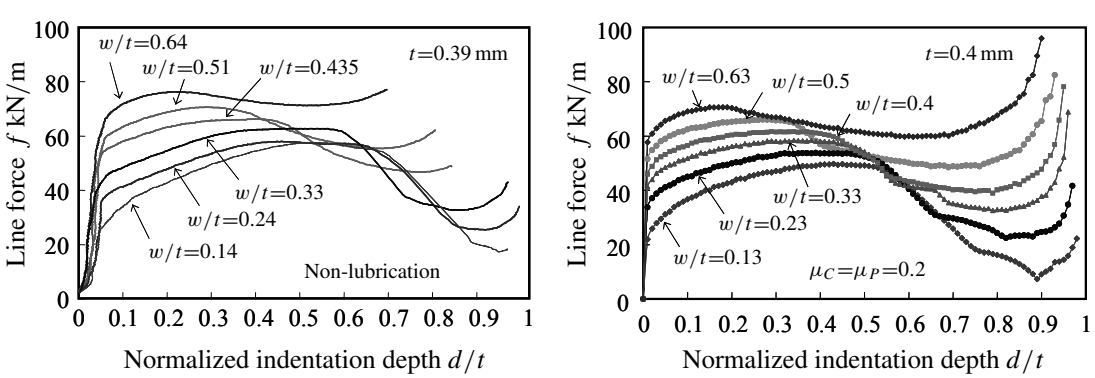

(a) Experiment ($w/t = 0.14 \sim 0.64$) (b) FEM simulation ($w/t = 0.13 \sim 0.63$)

Figure 3. Relationship between line force and normalized indentation depth.

3.1. ***Relationship between resistance of blade indentation and tip thickness.*** Figure 3a–b shows the experimental and FEM simulation of the relationship between the line force f and the normalized indentation depth d/t for $w/t = 0.14, 0.24, 0.33, 0.43, 0.51$ and 0.64. The tendency of the load response in the FEM simulation was very similar to that of the experiment result. Figure 4a illustrates a force response model that includes cutting characteristics of Figure 3, where f_n is an inflection point of f and f_u is a local minimum point of f, as defined in [Murayama et al. 2004]. The maximum load point is denoted by $(f_{\max}, d_{\max}/t)$, where $f_{\max}$ is the line force, and $d_{\max}$ is the corresponding indentation depths of the blade.

Figure 5a shows the dependency of $f_{\max}$, f_n and f_u on normalized tip thickness w/t in the experiment, while Figure 5b shows the dependency of $f_{\max}$, f_n and f_u on normalized tip thickness w/t in the FEM simulation for $\mu_P = \mu_C = 0.2$.

Since $f_{\max}$ was roughly linear to the variance of w/t, approximations of $f_{\max}$ by the least squares method were derived as follows:

$$f_{\max} = 36.4(w/t) + 52.8\,\text{kN/m (experiment)} \tag{1}$$

$$f_{\max} = 43.4(w/t) + 44.3\,\text{kN/m (FEM)}. \tag{2}$$

The linear correlation coefficient R of (1) and (2) was 0.98 and 0.999, respectively. We supposed that the difference between (1) and (2) is mainly due to the assumption of the coulomb friction model. It is known that $f_{\max}$ decreases [Murayama et al. 2004] as μ_C decreases. Comparing the experimental f_n with Prandtl's theory $f_n = 2k(1+\pi/2)w$ [Hill 1983], where the shearing yield stress k was assumed to be $\sigma_{0.2}/\sqrt{3}$, f_n can be estimated as a flat punch indentation (Prandtl's solution) for $w/t < 0.23$, but not for $w/t > 0.23$, due to the Hill's critical thickness.

When the blade indentation increased, after passing through the maximum load point, the aluminum sheet separated into two pieces; otherwise the aluminum sheet only showed a locally minimum line force without any separation. In particular, for $d/t > d_{\max}/t$ for $w/t \geq 0.13$, the reduction stage of f had an

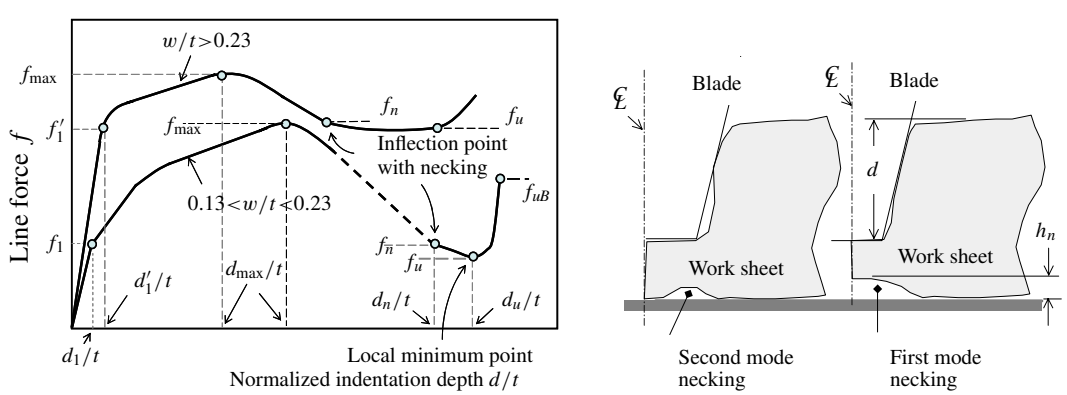

(a) Force response model (b) Necking deformation

Figure 4. Force response model for the indentation process; schematic of necking deformation.

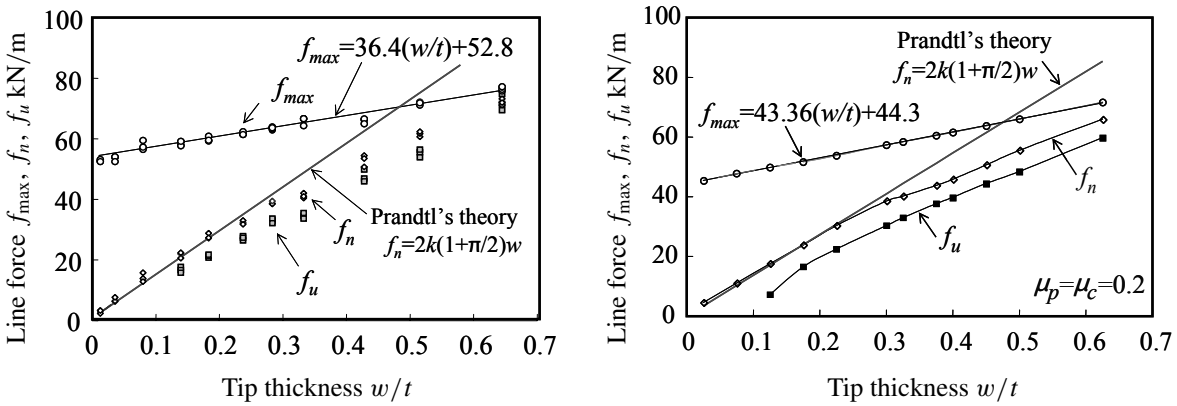

(a) Experiment (b) FEM simulation

Figure 5. Relationship between line forces and tip thickness.

inflection point $(d_n/t,\ f_n)$ and a local minimum point $(d_u/t,\ f_u)$ as shown in Figure 4a. For $w/t < 0.23$, [Murayama et al. 2004] defined the height of necking h_n and necking deformation as shown in Figure 4b. The inflection point $(d_n/t,\ f_n)$ corresponds to the maximum height of necking $(h_n = h_{\mathrm{nmax}})$.

Figure 6 shows the first inflection line force f_1 and f_1'. The first inflection point was tentatively classified as f_1 and f_1' from the disappearance condition of the second inflection point, depending on the critical thickness $w/t = 0.23$. Since f_n was almost equal to f_1 from both the experiment and the FEM simulation, and considering that they could be estimated by the Prandtl's theory for a flat punch

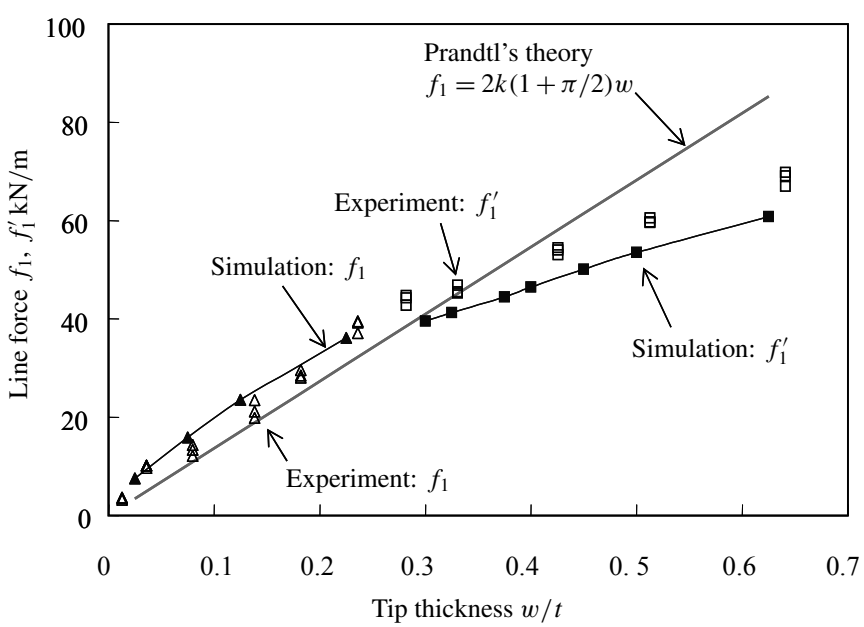

Figure 6. Variation of line force at first inflection point with respect to tip thickness.

indentation into a semi-infinite body [Hill 1983], we assumed that the wedge effect decreased and the upsetting effect increased at the inflection point $(d_n/t, f_n)$. In other words, the detaching phenomenon on the wedge surface of the blade seemed to occur at that time.

When f was equal to f_u, the bottom of the first necking zone contacted with the counter plate completely. When $w/t < 0.13$, f decreased for d/t without the local minimum point $(d_u/t, f_u)$. The local minimum point of f_u corresponded to $h_n = 0$, the occurrence of the second necking zone, and also the upsetting on the burr. When $w/t > 0.28$, the second necking did not occur, but the first necking mode altered directly into the upsetting mode. Also, the local minimum point $(d_u/t, f_u)$ corresponded to detaching the wedge surface from the worksheet and upsetting with the blade tip. The correlation between $(d_n/t, f_n)$ and $(d_u/t, f_u)$ was confirmed experimentally using the following approximations for $0.51 > w/t > 0.13$:

$$f_u = (0.36(w/t) + 0.75) f_n \tag{3}$$

$$d_u = (0.46(w/t) + 0.99) d_n. \tag{4}$$

The linear correlation coefficient R for relations (3) and (4) were 0.815 and 0.926, respectively. When $w/t > 0.5$, the line force response does not include a sharply breaking down flow process. This tendency may be due to detaching of the wedge surface of the blade.

So far, detachment of the wedge surface under upsetting, the local minimum load point, and the inflection load point with the second necking on the second half stage $(d > d_{\max})$ are important for estimating wedging separation of the aluminum worksheet. However, in past studies, the position of any inflection points on the second half stage and a transformation mechanism from the second necking to upsetting were not discussed with respect to the detaching condition. Therefore, in the following sections, we shall discuss the deformation mode and the detaching condition.

3.2. ***Effect of deformations of a wedged sheet and tip thickness on the final stage.*** The contact condition between the sliding surface of the trapezoidal cutting blade and the deformed aluminum work sheet on the second half stage $(d/t > d_{\max}/t)$ is analyzed here by observing both experimental photographs of the wedged aluminum sheet, and deformation in the FEM simulation. Figure 7 shows SEM micrographs of the wedged profile of the aluminum work sheet near the local minimum load point for $w = 14, 92, 129$ and $200\,\mu$m, $t = 0.39$ mm, and $\alpha = 42$ degrees. By examining the bottom surface of specimens for $w/t = 0.013 \sim 0.079$, we observe that the first necking mode occurred near the blade tip, and the aluminum sheet successfully separated into two pieces without any burr.

In the experiment, where $0.28 > w/t > 0.13$, second necking mode was observed after occurrence of the first necking mode. A burr occurred near the local minimum load point without final bursting of the worksheet in the region between the blade tip and the counter plate Figure 7b. However, for $w/t = 0.13 \sim 0.28$, by increasing the line force to the breaking line force f_{uB}, the burr was likely to be broken, or the aluminum worksheet frequently separated into two pieces. f_{uB} was roughly equal to f_n at $w/t = 0.14$, whereas it was nearly $f_{\max}$ at $w/t = 0.24$. Throughout the experiment, we confirmed that the aluminum worksheet was not completely separated for $w/t > 0.28$ when the indentation depth exceeded the local minimum load point. Under these conditions, only the upsetting deformation of the worksheet occurred beneath the blade tip, even when applying a line force f larger than $f_{\max}$.

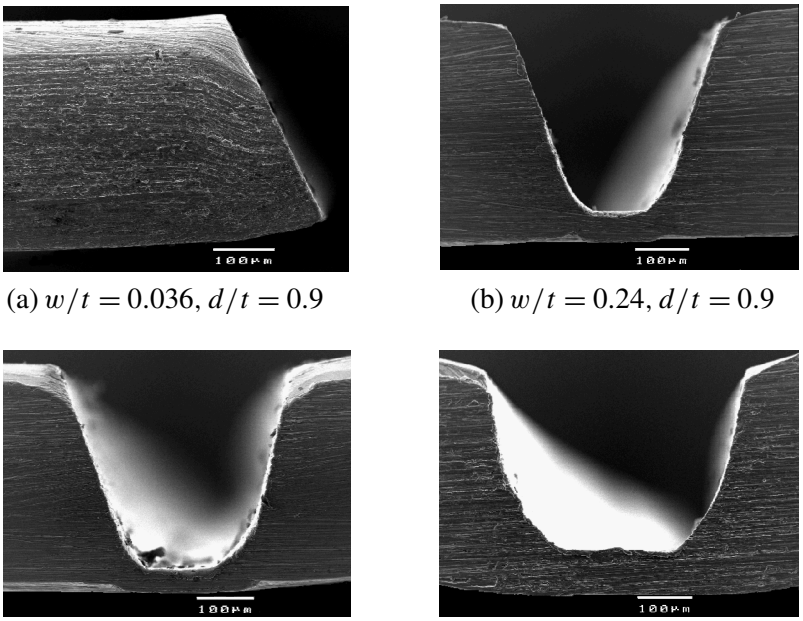

(a) $w/t = 0.036$, $d/t = 0.9$ (b) $w/t = 0.24$, $d/t = 0.9$

(c) $w/t = 0.33$, $d/t = 0.9$ (d) $w/t = 0.51$, $d/t = 0.7$

Figure 7. Wedged profile of aluminum worksheet (experiment).

Figure 8 shows an example of a wedged worksheet burst at $f_{uB} = 42$ kN/m on $w/t = 0.18$. Here, there was a round-shaped surface on both sides Figure 8b. There were two kinds of surfaces: the sheared zone and the drawing zone. The sheared zone is flat and seems to be formed by copying the profile of the blade edge. The drawing zone is round-shaped and seems to be formed by the extrusion effect of the blade tip pressure. Since this extrusion effect causes material flow in the outward lateral direction, we consider that the detached zone occurs beneath the wedge surface. We observed similar surfaces for $w/t > 0.24$(Figure 7b–d). Therefore, the surface of the wedge corner is considered to be detached from the deformed worksheet. On the other hand, when $w/t = 0.036$, the wedged surface of the worksheet appeared to be in contact with the blade edge. For $w/t = 0.33$ and $d/t = 0.75$, the second necking mode was not observed. Only the upsetting deformation was generated beneath the tip blade. When $w/t = 0.51$, $d/t = 0.7$, the wedge surface of the blade is completely detached from the work sheet and the upsetting flow occurred beneath the blade tip without any necking of the bottom surface.

Figure 9 shows the probability of the occurrence of separation of the wedged aluminum sheet. Experiments were carried out on 10 specimens for each tip thickness w of the blade. The indentation of the blade was stopped at the breaking line force f_{uB}, which exceeded the local minimum load point $(d_u/t,\ f_u)$, but was less than the maximum line force $f_{\max}$. The experimental probability p of separation was 100% for $w/t < 0.079$, but an intermediate value ($0 < p < 100\%$) for $0.14 < w/t < 0.23$. When the worksheet was separated as $0 < p < 100\%$ for $0.14 < w/t < 0.23$, the separated edge of the worksheet had a burr, as shown in Figure 8a.

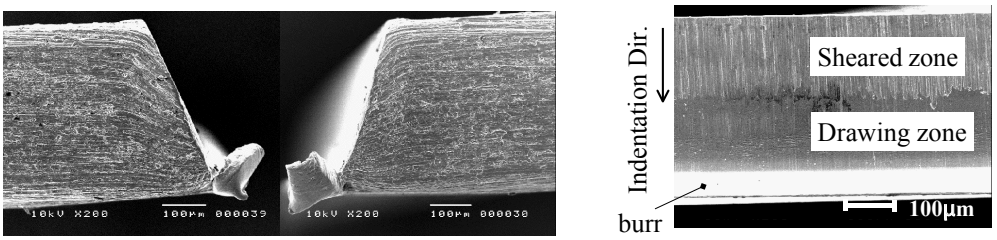

(a) Sectional view of both sides (b) Front view of a wedged surface

Figure 8. Wedged profile of aluminum worksheet ($w/t = 0.18$, $f_{uB} = 42$ kN/m in experiment).

Figure 10 shows a section profile of the wedged worksheet in the FEM simulation for $w = 10, 90, 130$ and $200\,\mu$m. Comparing Figure 10 with Figure 7, the simulated deformation of the worksheet shows good agreement with experimental observation.

By referring to this figure, we can confirm the following four main points. First, for $w/t = 0.025$, only the first necking mode was observed for $d/t = 0.7, 0.9$. Second, for $w/t = 0.23$, the first necking mode at $d/t = 0.7$ altered to the second necking mode at $d/t = 0.9$. Third, when $w/t = 0.33$, the first necking mode at $d/t = 0.6$ altered to the upsetting mode without the second necking at $d/t = 0.85$. Fourth, when $w/t = 0.5$, only the upsetting deformation was generated beneath the blade tip for $d/t = 0.6, 0.7$.

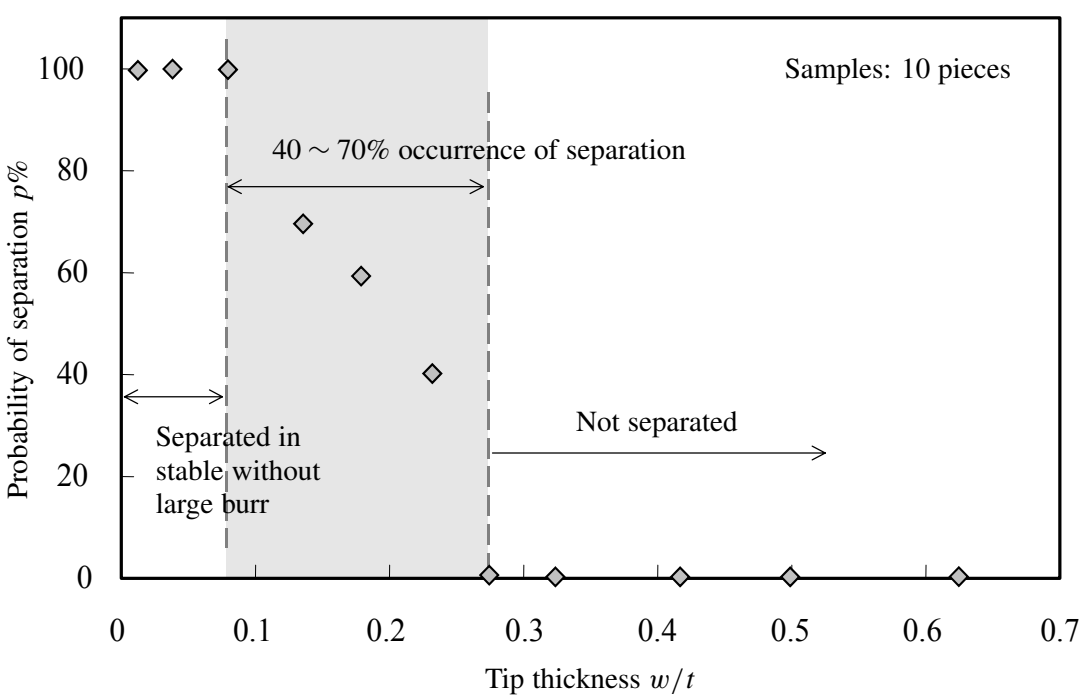

Figure 9. Probability of separation (experiment).

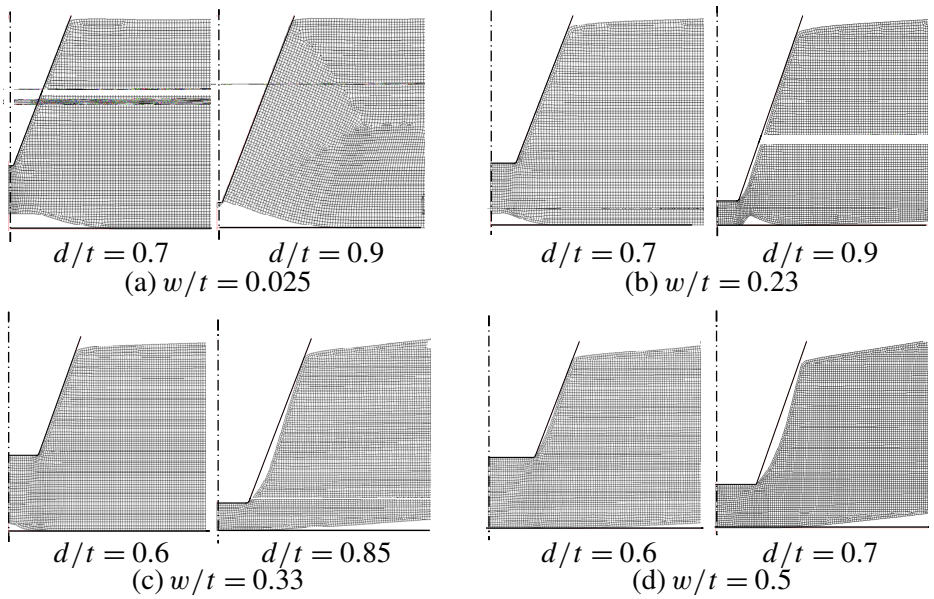

Figure 10. Wedged profile of worksheet on simulation.

In addition, the deformed surface of the worksheet was completely detached from the wedge surface of the blade near the inflection point $(d_n/t, f_n)$ for $w/t = 0.33$ and $w/t = 0.5$. Where $w/t = 0.33$ and $w/t = 0.5$, upsetting flow of the worksheet was generated beneath the blade tip without any separation in the final stage. Therefore, we confirmed that both the detached condition on the sliding surface and the probability of separation of the blade depend on w/t.

3.3. ***Effect of detached/contact length and indentation depth on an edge of cutting blade.*** As mentioned in the previous section, the occurrence of a detached zone relates to the possibility of wedge separation. We investigate here the effect of detached length a_d and contact length a_c on the wedge surface as defined in Figure 2b. The detached length a_d and the contact length a_c were considered to be the projected length of the free surface on which $p_m = 0$, and the pressurized surface on which $p_m \neq 0$, respectively. p_m is defined as the normal pressure on the wedge surface of the cutting blade. The complete-open condition is that which occurs when the wedge surface is completely detached from the work material. After reaching the complete open condition, the detached length a_d is redefined as the projected length from the blade's edge to the end of the wear zone of the work sheet.

Figure 11 shows the normalized detached length $a_d/(t/\cos(\alpha/2)$, which was numerically calculated, and the normalized contact length $a_c/(t/\cos(\alpha/2)$ obtained by varying d/t with respect to $w/t = 0.13$. The closed square symbols show normalized contact length $a_c/(t/\cos(\alpha/2))$, while the open round symbols show normalized detached length $a_d/(t/\cos(\alpha/2))$. In Figures 11–12, the symbol a denotes the total contact and detached length $(a_c + a_d)$, contact length a_c, or detached length a_d. The solid line represents the normalized total projection of contact and detached length $(a_c + a_d)\cos(\alpha/2)/t$, while the dashed line is the ideal indentation depth (d/t). The normalized total projection length $(a_c + a_d)\cos(\alpha/2)/t$, which excludes the wear curve on sliding surface, is slightly smaller than that of the ideal indentation

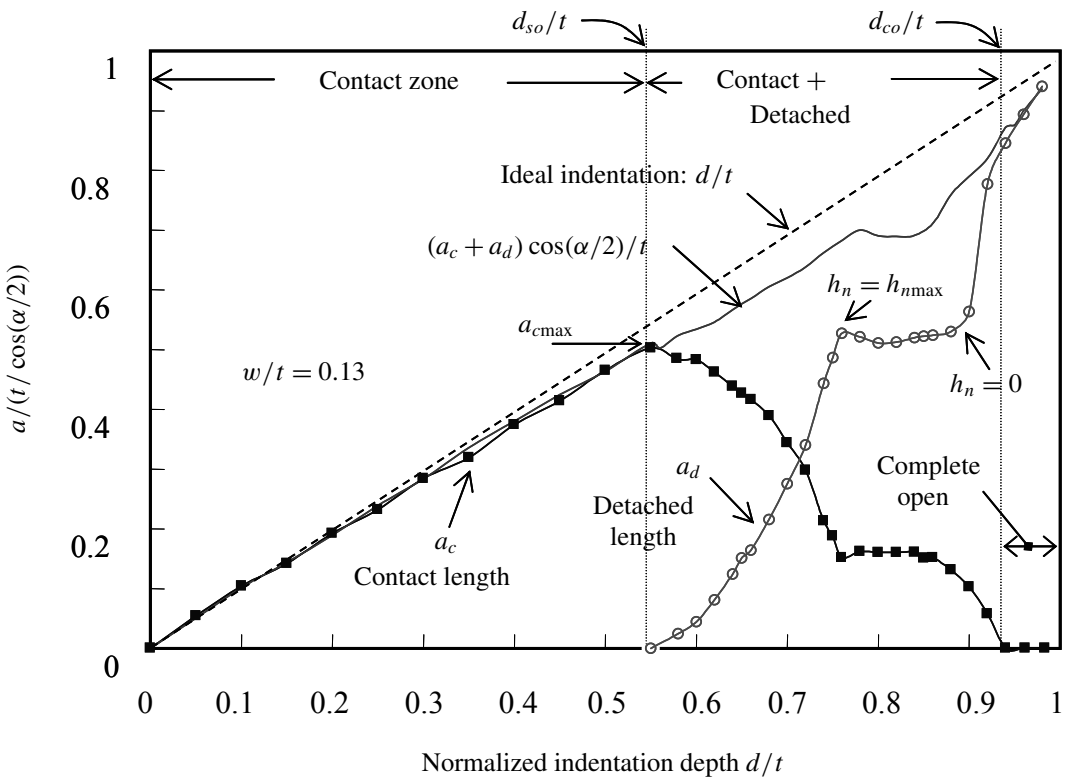

Figure 11. Relationship between detached/contact length and normalized indentation depth d/t.

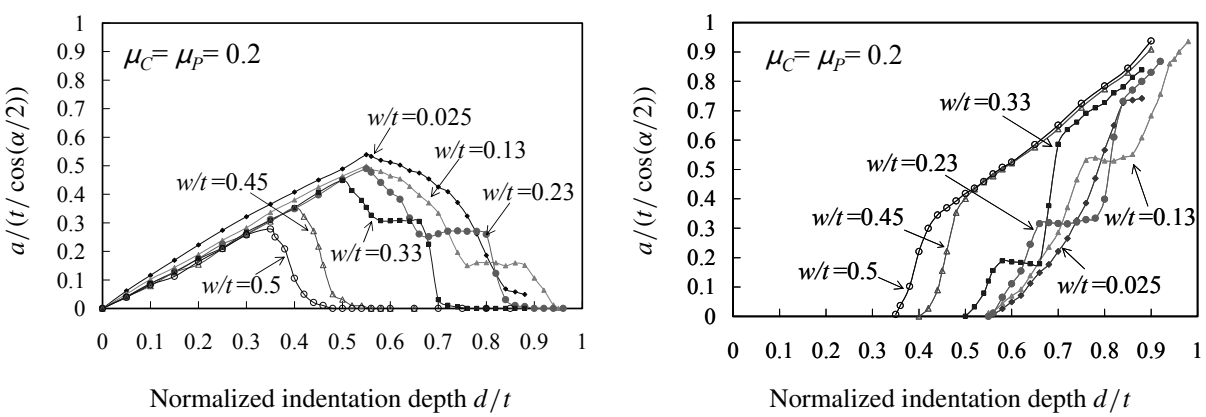

(a) Contact length

(b) Detached length

Figure 12. Effect of tip thickness w/t on the occurrence of contact length and detached length on simulation.

depth. We defined the first half stage $d/t = 0 \sim 0.55$, as the contact zone, since only the contact part was observed on the wedge surface. When a_c reaches the maximum peak value a_{cmax}, the detached length a_d began to appear at $d/t = d_{so}/t$ and increased with increasing indentation depth. We define the contact + detached zone as that which a_c then decreases to zero. From these relations, we found that the position of a_{cmax} is nearly equal to the starting position of the detached zone. In addition, the maximum height of the first necking h_{nmax} was observed at $d/t = 0.76$, and with respect to $w/t = 0.13$, the bottom of the necking zone started to contact with the counter plate at $d/t = 0.88$ ($h_n = 0$ at this point). As the height h_n of the first necking mode decreased, the values of a_d and a_c were almost constant. When a_c reaches zero at $d/t = d_{co}/t$, the wedge is completely detached from the deformed worksheet. Thus far, we denote the critical depth d_{so} as the lower-bound position of the detaching phenomenon, and the critical depth d_{co} as the upper-bound position of the detaching phenomenon.

Assuming $n = 0.08$ and $F = 224$ MPa (Table 1), we considered the transverse direction model in the FEM simulation. Comparing the FEM simulation in the transverse direction of the material worksheet with that in the longitudinal direction, we confirmed that the detaching phenomena characterized by a_d, a_c was almost the same with respect to w/t and d/t, except for the magnitude of the cutting line force.

Figures 12a and b show the effect of w/t on variation of the contact length and detached length. When $w/t < 0.1$, the wedge surface is contacted with a specific sliding surface area of the deformed aluminum sheet. However, we did not observe an inflection point of a_c for $w/t > 0.4$. This is because the upsetting flow only occurred beneath of the blade tip without the second necking mode.

3.4. ***Effect of friction coefficients on cutting load response and detached condition.*** The effect of line force f, indentation depth d/t, and the corresponding contact/detached length a_c, a_d on the wedge surface are analyzed here by varying the friction coefficients μ_P, μ_C for $w/t = 0.13$. Figure 13a shows the relationship between f and d/t for friction coefficients $\mu_P = 0.0, 0.1, 0.2$, and 0.4, with $\mu_C = 0.2$. Figure 13b shows the relationship between a_c, a_d, and d/t. Similarly, Figure 13c shows the relationship between f and d/t for $\mu_P = 0.0, 0.1, 0.2$, and 0.4, with $\mu_P = 0.2$, while Figure 13d shows the relationship between a_c, a_d and d/t.

From these figures, we observe that f_{max} and a_{cmax} depend on the variation of μ_C, μ_P, as shown in the approximations

$$\begin{aligned} f_{\text{max}} &= 18.6\mu_P + 46.1 && \text{for } \mu_C = 0.2 \\ a_{\text{cmax}} &= 0.234\mu_P + 0.464 && \text{for } \mu_C = 0.2 \\ f_{\text{max}} &= 43.8\mu_C + 40.3 && \text{for } \mu_P = 0.2 \\ a_{\text{cmax}} &= 0.282\mu_C + 0.455 && \text{for } \mu_P = 0.2. \end{aligned} \tag{5}$$

The linear correlation coefficients of (5) were larger than 0.99. The inflection position ($h_n = h_{\text{nmax}}$) and the lower/upper-bound position d_{so}, d_{co} almost did not depend on μ_P, while the d_{so}, d_{co} depended on μ_C. The responses of a_c and a_d with d/t also depended on μ_C, μ_P, except for the complete open condition. Therefore, we can confirm that the variation of μ_C, μ_P affects the line force and also the detached condition. Furthermore, the effect of variance of μ_C was relatively large.

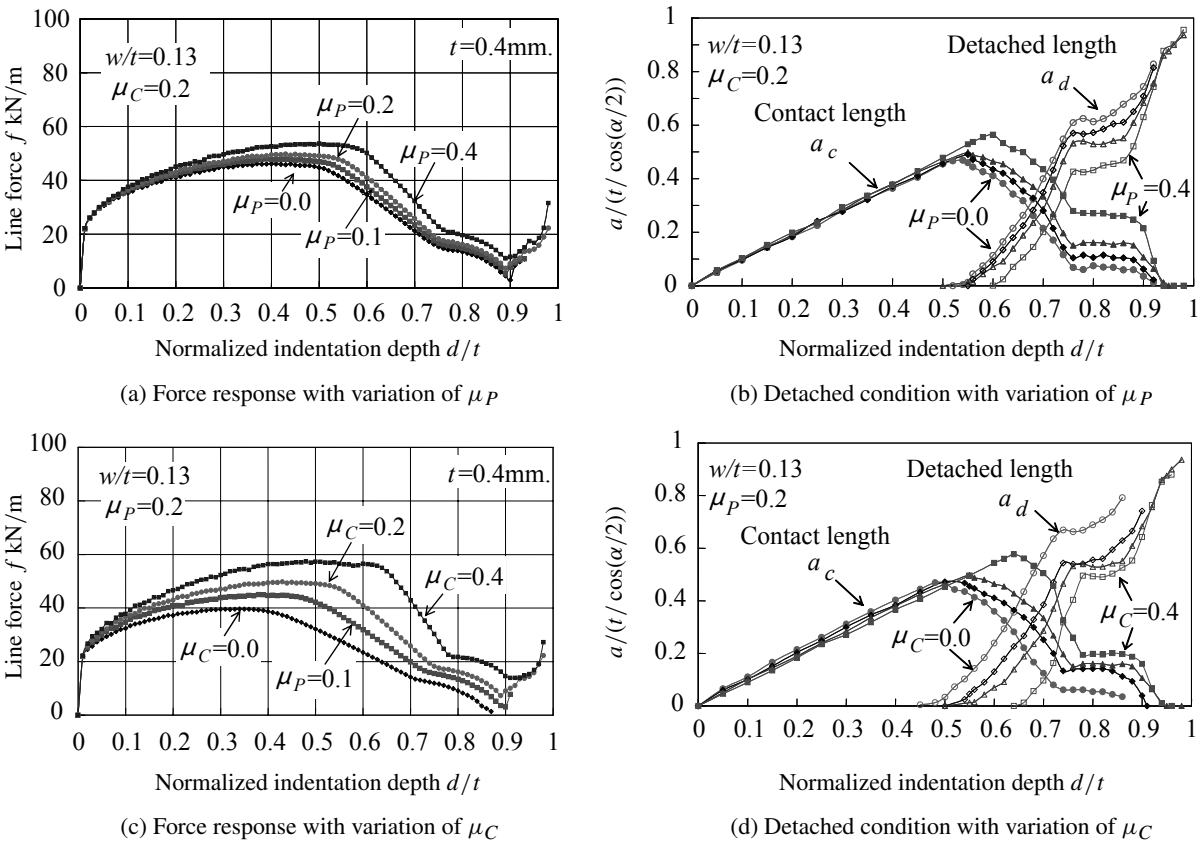

(a) Force response with variation of μ_P

(b) Detached condition with variation of μ_P

(c) Force response with variation of μ_C

(d) Detached condition with variation of μ_C

Figure 13. Effect of friction coefficient for load response and detached condition on simulation.

3.5. ***Stress distribution in the necked zone on the final stage.*** As mentioned in section 3.2, the probability of the occurrence of separation had the intermediate experimental value ($0 < p < 100\%$) for $0.14 < w/t < 0.23$. In this section, we discuss the stress distribution around the blade tip. Figure 14 shows contour bands of maximum principal stress σ_{pmax} beneath the blade tip at $d/t = 0.9$, while Figure 15 shows those of maximum shear stress τ_{max} at $d/t = 0.9$ by the FEM simulation. Figure 16 illustrates selected vectors of principal stresses chosen near the necked zone. When $w/t = 0.13$, the maximum stress as the principal component was roughly $\sigma_{\text{pmax}} = 320$ MPa (tensile) in the second necking zone, where the minimum dimension was roughly 17% of the chip height. For $w/t = 0.23$, the minimum dimension of the necked zone was roughly 102% of the chip height. The absolute value of σ_{pmax} was relatively small (less than 100 MPa) in the necked zone but increased remarkably as a compressive component beneath blade tip.

Figure 17 shows the distribution of σ_{pmax} along the specified nodes path $X' - X$, at $d/t = 0.9$. Here, the arc distance a_L was measured as the distance from the corner of the blade tip to the necked surface for $w/t = 0.13, 0.18$, and 0.23, while the a_L was considered from the corner of the blade tip to the bottom surface of the work sheet for $w/t = 0.3$ and 0.5. When $w/t = 0.13$, the maximum value of σ_{pmax}

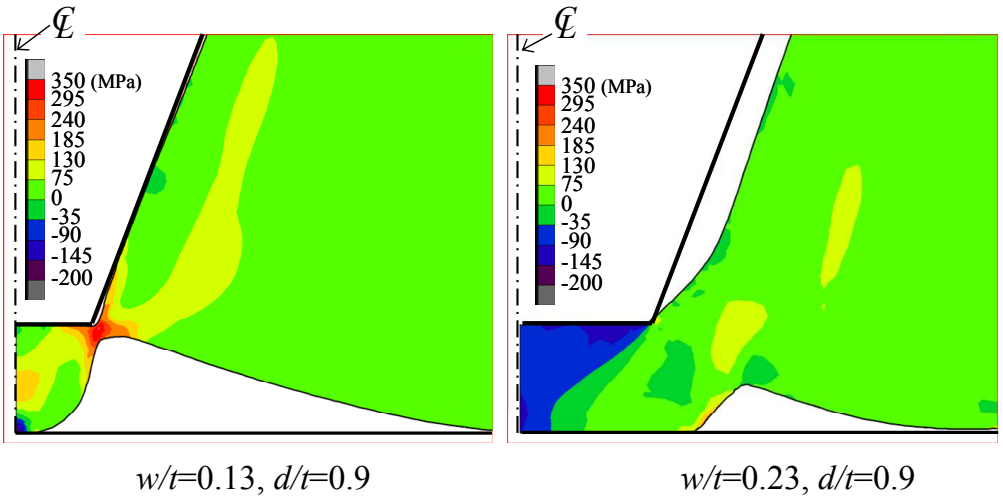

Figure 14. Calculated contour bands of maximum principal stress in wedged worksheet at $d/t = 0.9$.

was roughly 320 MPa and the $\tau_{\max}$ was larger than $\sigma_{0.2}/\sqrt{3}$ in the necked zone. Applying the maximum tensile strength of the aluminum sheet to σ_B, $\sigma_{\text{pmax}} \approx 2\sigma_B$, the worksheet would actually be separated. When w/t increased, σ_{pmax} was intensively compressive near the corner of the blade tip, and its absolute value was less than 50 MPa for $w/t > 0.3$. Therefore, it seemed that the aluminum worksheet could not be separated for $w/t > 0.23$. This result was in good agreement with experimental results.

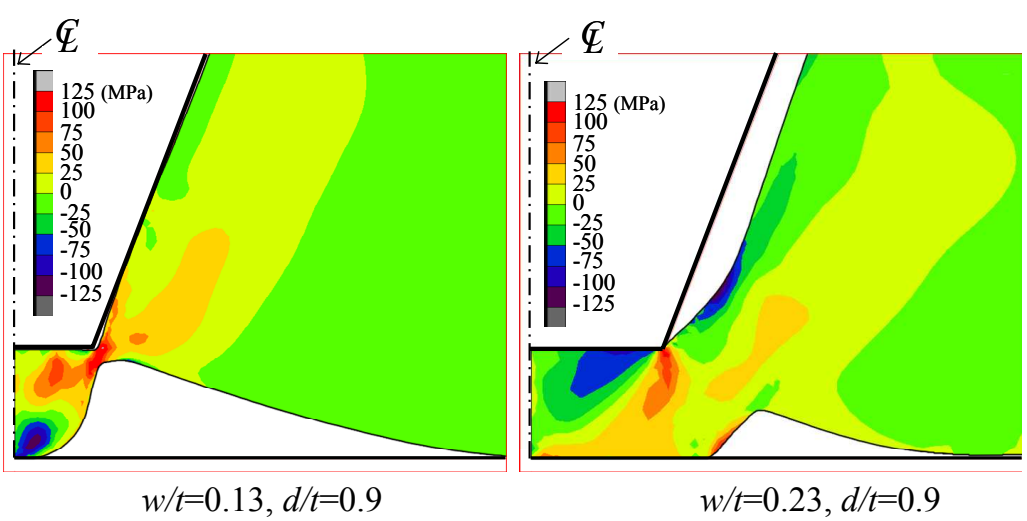

Figure 15. Calculated contour bands of maximum shear stress in wedged worksheet at $d/t = 0.9$.

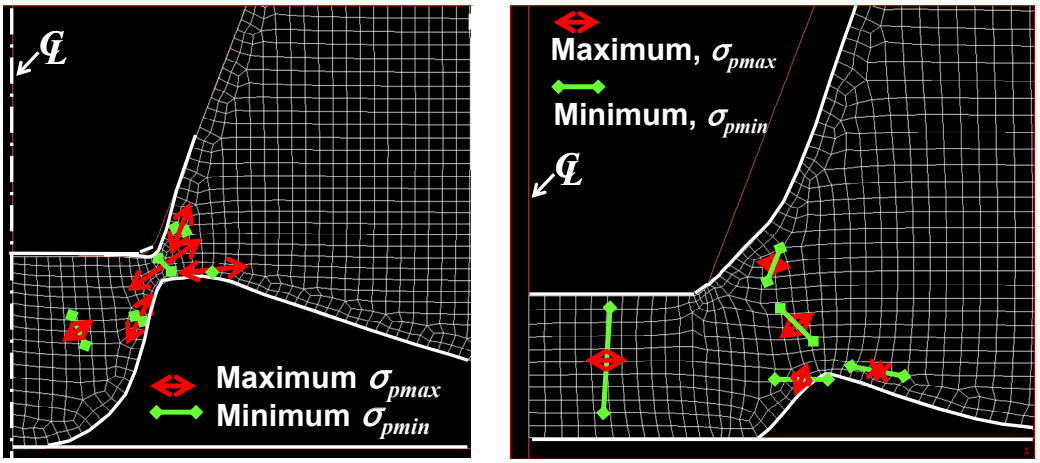

(a) w/t =0.13 (b) w/t=0.23

Figure 16. Calculated vectors of principal stresses at $d/t = 0.9$.

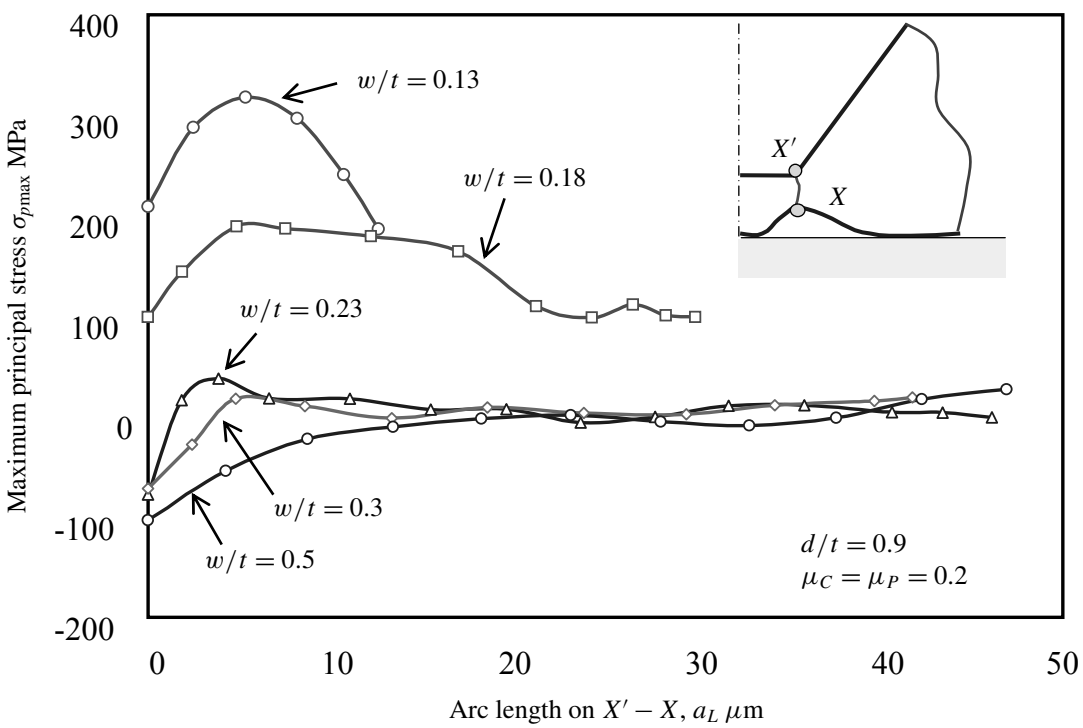

Figure 17. Distribution of maximum principal stress in $X' - X$ at $d/t = 0.9$ by varying w/t.

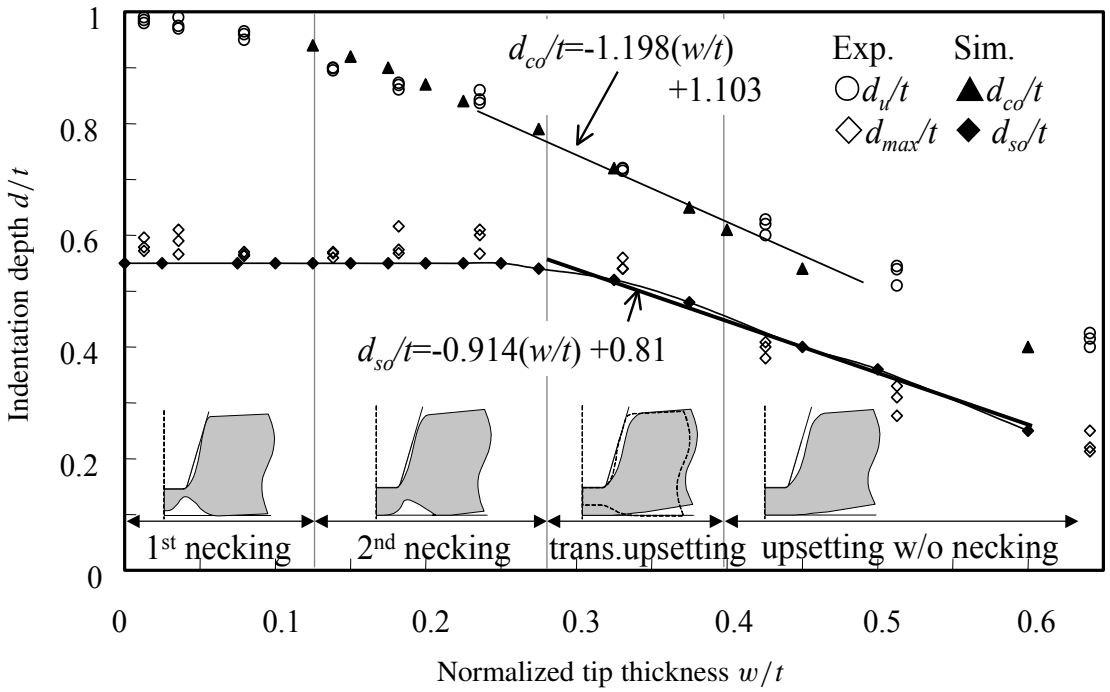

Figure 18. Relationship between indentation depth d_{so}, d_{co} at critical detaching condition and tip thickness.

3.6. ***Relationship between critical indentation depth of the detached condition and tip thickness.*** Figure 18 shows the lower bound detaching position d_{so}/t, and the upper bound detaching position d_{co}/t derived from the detached length of the wedged surface by FEM simulation. Schematics of the deformed worksheet are also illustrated, showing four deformation modes: first necking, second necking, the transition state and the upsetting mode. The open squares and circles show experimental results $d_{\max}/t$ and d_u/t obtained by varying w/t, while the closed squares and triangles show the numerically derived d_{so}/t and d_{co}/t, respectively. Comparing these values, we confirm that the position of the maximum load point $d_{\max}/t$ corresponds to the initial detached position of d_{so}/t, while the position of the local minimum load point d_u/t is related to the complete-detached position d_{co}/t. Therefore, the position of the maximum line force $f_{\max}$ and the position of the local minimum line force f_u are useful for estimating the detached position d_{so}/t and d_{co}/t, respectively.

For $w/t = 0 \sim 0.28$, d_{so}/t was nearly constant at 0.55. When $w/t > 0.28$, d_{so}/t began to decrease linearly as

$$d_{so}/t = -0.914(w/t) + 0.81 \text{for } w/t > 0.28 \tag{6}$$

When $w/t > 0.13$, d_{co}/t decreases with w/t as

$$d_{co}/t = -1.198(w/t) + 1.103 \qquad \text{for } w/t > 0.13. \tag{7}$$

Only if $w/t < 0.13$ does the wedge surface always contact some part of the deformed aluminum sheet.

From the above discussion of Figure 18, we classified the pushing shear condition of the aluminum worksheet into the following four features derived from both the detached length on the wedge surface and from the load response:

1) When $0 < w/t < 0.13$, the first necking mode was observed and the wedge surface was in contact in some area of the aluminum sheet. In this stage, the work material is completely separated without any burrs.
2) When $0.13 < w/t < 0.28$, the second necking mode of the bottom surface occurred in the second half stage ($d/t > d_{\text{max}}/t$), while the first necking mode was generated in the first half stage ($d/t < d_{\text{max}}/t$). Lower-bound detaching on the wedge surface and upper-bound detaching on the wedge surface are observed under this condition. The blade is statistically able to separate the worksheet with a burr.
3) When $0.28 < w/t < 0.4$, upsetting deformation is generated after occurrence of the transient first necking mode. The wedge surface is always detached from work material in the final stage.
4) When $w/t > 0.4$, the plain upsetting mode without any necking always occurred beneath the tip blade. Specifically, the apex angle of the wedge is not effective to cut off the worksheet.

3.7. ***Relationship between separation line force and indentation depth in the simulation.*** Figure 19 describes the numerically calculated relationship between a separation line force f_s and the normalized indentation depth d/t obtained by varying the tip thickness w/t. f_s is a lateral component of the applied line force to the worksheet. It was obtained using a line integral of the normal stress σ_{xx} (the horizontal component) on the center line, from the bottom surface of the work material to the blade tip surface. Figure 19 shows three peaks, or inflection points ($f_{\text{smax}}, d_{\text{smax}}/t$), ($f_{sn}, d_{sn}/t$), and ($f_{su}, d_{su}/t$). When $f_s = f_{\text{smax}}$, d/t was almost constant (approximately 0.55 for $w/t < 0.25$), while it decreased for $w/t > 0.25$. The position d_{smax}/t corresponded to the lower-bound detaching position of depth d_{so}/t. When $h_n = h_{\text{nmax}}$, f_s became the local minimum f_{sn}, and when $h_n = 0$, f_s became the second peak position f_{su} which corresponds to the upper-bound detaching position.

However, the two peaks or inflection points f_{sn}, f_{su} were not observed for $w/t > 0.4$, which corresponded to the dissipation of the first necking mode. The position depth of d_{sn}/t and d_{su}/t correspond to the position $h_n = h_{\text{nmax}}$ and the position $h_n = 0$, respectively. In Figure 19, the cross point of the x-axis of the f_s curve corresponds to the complete open position. For $w/t < 0.13$, f_s does not intersect with the x-axis at the final stage of indentation. That is, the separation force is always positive at the final stage.

4. Conclusions

Indentation of the trapezoidal cutting blade to an aluminum sheet was carried out experimentally and numerically to investigate the separation mechanism and its critical processability. The trapezoidal blade simulates the crushed wedge of a 42 degree center bevel blade. The detaching condition of the wedge

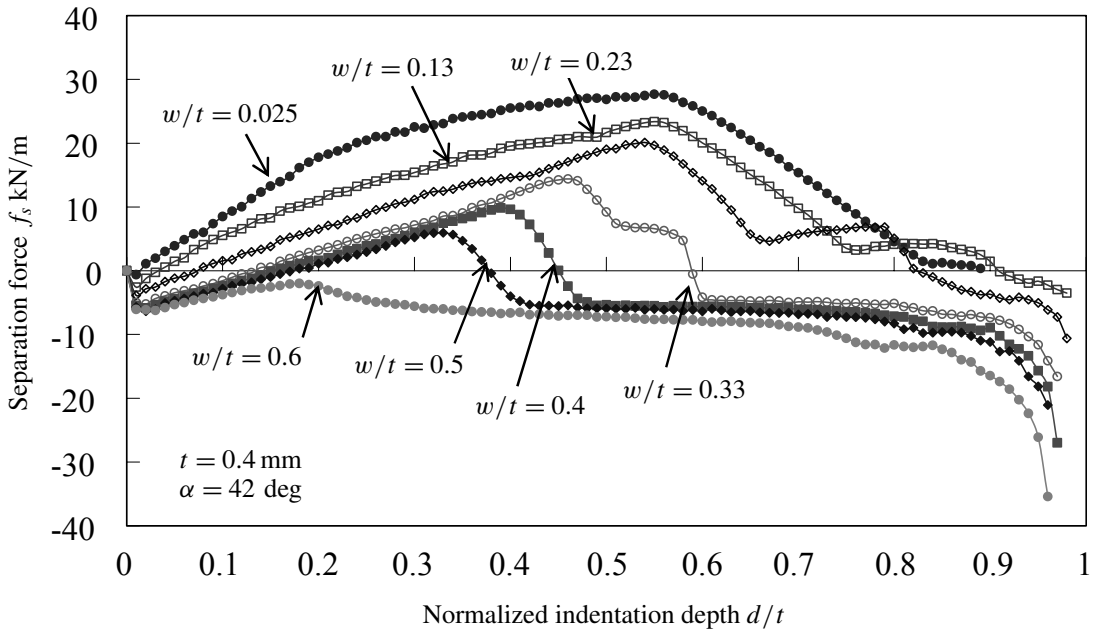

Figure 19. Relationship between separation line force f_s and d/t (simulation).

surface and the separation force were analyzed to explain the mechanism and the critical conditions which enable successful separation of a thin work sheet. Features of the deformation mechanism after occurrence of the detaching phenomenon were revealed as follows:

1) The wedged profile of the worksheet under the pushing shear can be classified into four patterns in terms of normalized tip thickness w/t. The first pattern is under sharp and fine conditions. When $w/t < 0.13$, the worksheet is successfully cut off without burrs or string-like chips. The second pattern is in the transition state of cutting. When $0.13 < w/t < 0.28$, a burr is generated and separation of the wedged sheet is statistically successful, although the probability of separation depends on w/t. The third pattern, where ($0.28 < w/t < 0.4$) and the fourth pattern, where ($w/t > 0.4$) ,occur under unsuccessful cutting conditions. Due to the upsetting flow beneath the blade tip, the wedge surface detaches from the deformed work sheet. The third pattern includes the transient first necking mode in the first half stage of indentation, while the fourth is always in upsetting mode.

2) The maximum load point ($f_{\max}, d_{\max}/t$) and the local minimum (or inflection) load point ($f_u, d_u/t$) are characterized by the initial detaching and the complete-open condition. The detachment on the wedge surface of the blade occurs in the transition state from the lower bound point, also called the initial detaching point, through the upper-bound point, or complete open state.

3) It is useful to observe the separation line force to explain necking of the wedged zone and detachment on the wedge surface of the blade.

4) Maximum contact length occurs near the initially detached position of indentation depth.

5) In the second necking mode, for the duration of the decrease in height of the necking root, the contact length a_c and the detached length a_d remain almost constant. The separation line force also remains approximately constant.

References

[Grebe and Hofer 1973] W. Grebe and H. Hofer, "Praktische Hinweise zur Schonung der Messer in Bandstahl Werkzeugen", *Papier-verarbeitung und Druck* **9** (1973), 292–300.

[Grunzweig et al. 1954] J. Grunzweig, I. Longman, and N. Petch, "Calculations and measurements on wedge-indentation", *J. Mech. Phys. Solids* **2**:2 (1954), 81–86.

[Hesse and Tenzer 1963] F. Hesse and H. J. Tenzer, "Grundlagen der Papier-verarbeitung", pp. 58–60 in *VEB Verlag fur Buch und Bibliotheks-wesen*, Leipzig, 1963.

[Hill 1953] R. Hill, "On the mechanics of cutting metal strips with knife-edged tools", *J. Mech. Phys. Solids* **1**:4 (1953), 265–270.

[Hill 1983] R. Hill, *The mathematical theory of plasticity*, Clarendon Press, Oxford, 1983.

[Inaba 1998] Y. Inaba, "Flatbed diecutting and maintenance of diecutter", *Carton Box* **17**:200 (Oct 1998), 17–20. In Japanese. Translated in Proceedings of Third Diecutting Symposium (Tokyo, 1998), pp. 15–19.

[MSC 2003] MSC Software, *Marc: theory and user information*, Santa Ana, CA, 2003.

[Murayama et al. 2003] M. Murayama, S. Nagasawa, Y. Fukuzawa, and I. Katayama, "Effect of sheet thickness and friction on load characteristic of crushed center bevel cutter indented to aluminum sheet", pp. 115–124 in *Computational methods in contact mechanics, VI*, edited by C. A. Brebbia, Trans. Wessex Inst. Eng. Sci. **38**, WIT Press, Ashurst, UK, 2003.

[Murayama et al. 2004] M. Murayama, S. Nagasawa, Y. Fukuzawa, and I. Katayama, "Cutting mechanism and load characteristic of trapezoidal center bevel cutter indented on aluminum sheet", *JSME Int. J. C: Mech. Syst. Mach. Elem. Manuf.* **47**:1 (2004), 21–28.

[Nagasawa et al. 2001] S. Nagasawa, H. Sato, D. Yamaguchi, Y. Fukuzawa, I. Katayama, and A. Yoshizawa, "Effects of tip clearance and blade hardness on cutting resistance and tip shape in paperboard die cutting", *J. Japan Soc. Technol. Plasticity* **42**:480 (Jan 2001), 38–42. In Japanese.

[Nagasawa et al. 2002] S. Nagasawa, Y. Fukuzawa, T. Yamaguchi, M. Murayama, D. Yamaguchi, and I. Katayama, "Effects of blade tip shape on thread dross occurrence in paperboard die cutting", *J. Japan Soc. Technol. Plasticity* **43**:498 (Jul 2002), 50–54. In Japanese.

[Nagasawa et al. 2004] S. Nagasawa, H. Sekikawa, M. Murayama, Y. Fukuzawa, and I. Katayama, "Effect of initial tip profile on crushing of center bevelled cutter – numerical analysis of crushing of cutter tip indented on paperboard", *J. Japan Soc. Technol. Plasticity* **45**:524 (2004), 747–751. In Japanese.

[Tanaka and Akamatsu 2001] Y. Tanaka and H. Akamatsu, "Development of testing system for cutting characteristics of pressure-sensitive adhesive tape", *Nitto Denko Technical Report* **39** (2001), 62–65. In Japanese.

Received 12 Jan 2006.

SEKSAN CHAIJIT: seksan@stn.nagaokaut.ac.jp
Graduate School of Information Science and Control Engineering, Nagaoka University of Technology, Nagaoka, Niigata, 940-2188 Japan

SHIGERU NAGASAWA: snaga@mech.nagaokaut.ac.jp
Department of Mechanical Engineering, Nagaoka University of Technology, Nagaoka, Niigata, 940-2188 Japan

YASUSHI FUKUZAWA: fukuzawa@vos.nagaokaut.ac.jp
Department of Mechanical Engineering, Nagaoka University of Technology, Nagaoka, Niigata, 940-2188 Japan

MITSUHIRO MURAYAMA: *Faculty of Business Administration, Nagaoka University, Nagaoka, Niigata, 940-0828 Japan*

ISAMU KATAYAMA: *Katayama Steel Rule Die Co., Ltd., Tokyo, 162-0381 Japan*